Screw Dislocation-Induced Strengthening-Toughening Mechanisms in Complex, Layered Material: The case Study of Tobermorite

Ning Zhang[1], Philippe Carrez[2] and Rouzbeh Shahsavari[1,3,4*]

[1]Department of Civil and Environmental Engineering, Rice University, Houston, TX, 77005, USA

[2]Unité Matériaux et Transformations, CNRS UMR8207, Bât. C6, Université de Lille 1, Villeneuve d'Ascq, 59655, France

[3]Department of Material Science and NanoEngineering, Rice University, Houston, TX, 77005, USA

[4]Smalley Institute for Nanoscale Science and Technology

*Corresponding author email: rouzbeh@rice.edu

Abstract

Nanoscale defects such as dislocations have a profound impact on physics of crystalline materials. Understanding and characterizing the motion of screw dislocation and its corresponding effects on mechanical properties of complex, low symmetry materials has long been a challenge. Herein, we focus on triclinic tobermorite, as a model system and a crystalline analog of layered hydrated cement, and report for the first time how the motion of screw dislocation can influence the strengthening-toughening relationship, imparting brittle-to-ductile transitions. By applying shear loading in tobermorite systems with single and dipole screw dislocations, we observe dislocation jogs around the dislocation core, which increases the yield shear stress and the work-of-fracture when the dislocation lines are along [100] and [010] directions. Our results demonstrate that dislocation core acts as a bottleneck for the initial straight gliding to induce intra-laminar gliding, which consequently leads to significant improvement in mechanical properties. Together, the fundamental knowledge gained in this work on the role of motion of dislocation core on mechanical properties provide improved understanding of deformation mechanisms in cementitious materials and other complex layered systems, providing new hypotheses and design guidelines for developing strong, ductile, and tough materials.

Keywords: Tobermorite; Screw dislocation; Dislocation jog; Inter-laminar gliding, Strengthening-Toughening mechanism, Cementitious material

1. Introduction

Creating strong and tough materials has always been desired in various engineering applications.[1-4] Generally speaking, there exists two distinct approaches to improve the mechanical properties of materials: one involve chemical bonds interactions, such as the introduction of a metallic[5-7] or polymeric ductile phase[8-9] and the other involves optimization of physical structures, such as the hierarchical structure explored in nacre,[10-12] shape modulation [13-14] and molecular topology.[15]

In the context of engineered materials, Portland cement concrete is the most widely used material in the world, whose production and use contribute to 5-10% of CO_2 emissions worldwide and consumes a great deal of energy.[12] There is currently an urgent need for developing new concrete materials with greater specific mechanical properties and lower environmental footprints.[15-16] The key ingredient of concrete is cement, the glue and structural binder of concrete, whose hydration product is mainly Calcium-Silicate-Hydrate (C-S-H) phase. This phase is responsible for the important properties such as strength, stiffness and toughness of concrete.[17-18] There are also several naturally occurring C-S-H phases such as tobermorite minerals. So far, four members have been sufficiently characterized: clinotobermorite, tobermorite 9 Å, tobermorite 11 Å, and tobermorite 14 Å.[19] The particular interest in the structure and chemistry of tobermorite stems from its close relationships with C-S-H.[15] Therefore, with special consideration of tobermorite 11 Å for its central role in the family, broad studies have been carried on using various techniques and approaches with the goal of acquiring a deep knowledge of the structural aspects[19-22] and crystal chemical features[17, 23] of tobermorite minerals. It is widely accepted that C-S-H in Portland cement has a layered structure akin mostly to that of tobermorite.[23] Due to the similar crystal structure, tobermorite has been chosen as a basic model to create the database of atomic configurations for a wide range of C-S-H chemical compositions with various Calcium to Silicon (C/S) ratios vary from

~1.0 to ~2.5.[15] The layered tobermorite is found to be vulnerable to fracture on the interface between adjacent layers,[24] which indicates its brittle nature.[25]

It is well known that microscale defects including dislocation, crack, voids and impurities have significant influences on the chemical and physical properties of materials. In the past decades, great efforts have been undertaken to investigate[16, 26] and improve the mechanical properties of tobermorite.[8] Very recently, the effects of nanovoids and portlandite particles on balancing the strength and toughness of C-S-H were systematically studied by our group.[27] However, theoretical studies of dislocation properties in tobermorite have never been undertaken; despite the fact that dislocations, as the carriers of plasticity.[28] plays a key role in the deformation mechanisms and consequently governs the macroscopic mechanical properties.[29]

Dislocations can either form during deformation[13, 30] or prior to deformation.[28, 31-34] Mechanisms of dislocation movements are typically complex and can include double kink formation and square ring diffusion at the dislocation core.[28] Deformation of metals and alloys by dislocation gliding between separated planes is a well-understood process,[35] however, when it comes to more complex structures, knowledge of the detailed structure of dislocation core is quite essential to understand the deformation processes.[33] For example, numerical simulation reveals that when the stress is applied to drive the dislocation move, the dislocation core undergoes significant changes.[36-37]

Given the importance of dislocation in mechanical properties, improving our understanding of the atomic scale processes involved in dislocation migration will be a pre-requisite and crucial task in material science. However, so far, there is little prior work on modeling of dislocations in multi-element complex cementitious materials. To this end, research of dislocation motion in tobermorite at the nanoscale is essential for understanding and predicting its behavior and can provide new insights into the nature and mechanics of hydrated cement phases. Recently, our group investigated the core structure of screw dislocations and its impact on crystal growth of complex low symmetry oxides such as dicalcium

silicates.[32] While the results provided important information on unit processes of unhydrated cementitious materials, understanding the deformation mechanisms in real "hydrated" cement phases and potential dislocation climb including dislocation jog and kink remained unexplored. This is the key motivation behind this work.

Herein, we focus on two low index planes, (010) and (001), as the potential slip planes of tobermorite - a crystalline analog of C-S-H - and use molecular dynamics (MD) simulations as an "atomistic lens" to reveal the key deformation mechanisms and screw dislocation induced mechanical properties of tobermorite. To align our focus, we restrict this study to dislocation of purely screw characters (i.e. a dislocation line parallel to the Burgers vector of the defect). We introduce a single screw dislocation and dislocation dipole into tobermorite super cell, followed by applying pure shear loadings to drive the dislocation move. Our results demonstrate dislocation jogs and links and key strengthening-toughening relationships, which lead to improved strength and work-of-fracture in tobermorite. To the best of our knowledge, this is the first time that MD simulation has been used to study the effect of screw dislocation on mechanical properties of complex C-S-H materials such as tobermorite. The paper is organized as follows: section 2 briefly introduces the structure of tobermorite and details of dislocation introduction into tobermorite supercell. The simulation procedure is also described in this section. In section 3, we present and discuss the results of pure shear simulations, and finally conclusions are given in section 4.

2. Simulation Details

2.1 Structures of tobermorite with single screw dislocation and screw dislocation dipole

In this study, we focused on tobermorite 11 Å, which has a monoclinic crystal with calcium to silicon (C/S) ratio of 1.0. The lattice parameters are a=6.59 Å, b=7.39 Å, c=24.38 Å with $\alpha=\beta=90^0$, $\gamma=123^0$. Figure 1 displays the atomic representation of tobermorite. It is a layered mineral composed of a central Ca-O sheet with silicate tetrahedral chains flanking on both sides. The silicate chains are kinked with a periodicity of three tetrahedron[9] and follow a "dreierketten" or "wollastonite" -like chains.[20] Two of the

silicate tetrahedron share an oxygen and called paired tetrahedron while the third one acts as a connection between paired tetrahedron, so-called bridging tetrahedron (Figure 1). Water molecules and Ca cations, which determine the hydration degree and chemical composition, are located in the wide channel between pair silicate chains. Note that atoms can also be categorized as intra-laminar or inter- laminar atoms according to the gap between adjacent silicate chains,[15] as illustrated in Figure 1.

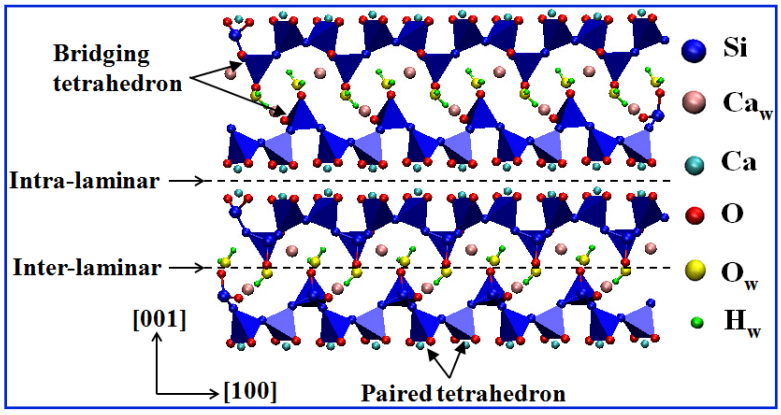

Figure 1. Side view of crystal structure of tobermorite. Ca_w, O_w and H_w denote the inter-laminar calcium, oxygen and hydrogen in water, respectively. The blue pyramids represent silicon tetrahedron.

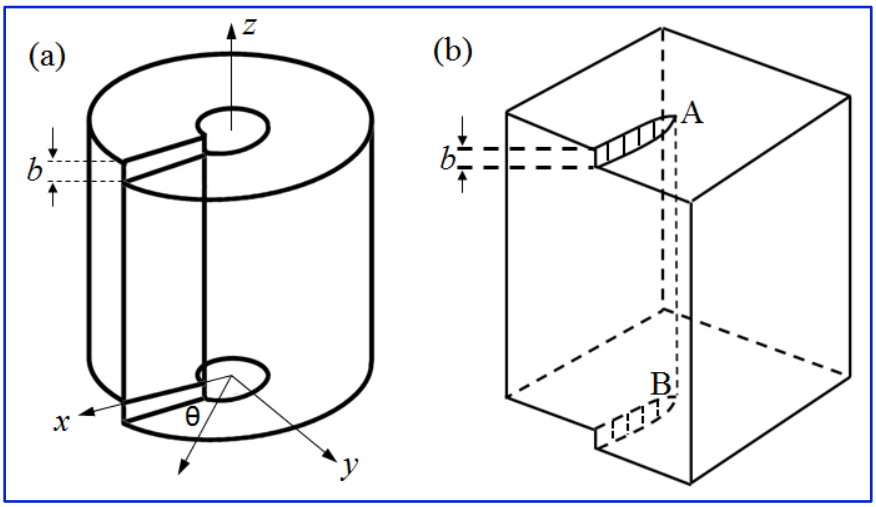

Figure 2. Schematic diagram of the introduction of a screw dislocation into an elastic body. (a) Voltaterra deformation mode; (b) a cubic sample with a screw dislocation. Burgers vector along dislocation line is denoted by ***b***.

The initial atomic structure of dislocation is created by using the classical isotropic elastic theory. To introduce a screw dislocation into an elastically isotropic body, a cut plane is created from the edge to the center. As defined by Volterra,[33, 38-39] the elastic distortion around a straight screw dislocation can be represented in terms of a cylinder of elastic material. Figure 2a presents the concept model of Volterra dislocation, in which the magnitude of Burger's vector of screw dislocation is *b* in the *z*-direction. For the elastic field in the dislocated cylinder (and in the supercell) (Figure 2a), it is noted that there are no displacement in the *x*- and *y*- directions while, in the *z*-direction, the displacement varies smoothly from zero to *b* as the angle θ goes from *0* to 2π. Therefore, the displacement field can be expressed as:

$$u_x = u_y = 0 \tag{1-a}$$

$$u_z = (b/2\pi)\times tan^{-1}(y/x) \tag{1-b}$$

where u_x, u_y, u_z are components of the displacement field around a dislocation; *x*, *y*, *z* are Cartesian coordinate. In Figure 2b, a screw dislocation running from *A* to *B* is introduced into a cubic sample by the elastic displacement field.

In the current work, screw dislocations both parallel and perpendicular to the calcium-silicate layers are introduced into tobermorite. A super cell with a cubic cross-section (10.0 nm × 10.0 nm in dimension) is generated first. The length of the tobermorite cuboid is controlled at 17.0 nm. The Burger's vectors of screw dislocation along [100], [010] and [001] are b_x = 6.59 Å, b_y = 7.39 Å and b_z = 24.38 Å, respectively. Burgers vector is the crystal vector that denotes the direction and magnitude of the atomic displacement that occurs when dislocation moves. Figure 3a-c present the computer models with dislocation lines along [001], [010] and [100], respectively. In addition, screw dislocation dipoles with opposite signs are also introduced into the super cell of tobermorite with dislocation lines along [001], [010] and [100], as shown in Figure 4a-c, respectively. The size of the super cell needs to be large enough to avoid core-core interaction due to the use of periodic boundary conditions in the glide plane. Therefore, in the present study, the dipolar screw dislocations are separated by a distance of 10.0 nm away from each other. It is

worth pointing out that to avoid cutting chemical bonds, the cut planes are chosen to be in between inter-laminar space during the introduction of screw dislocation.

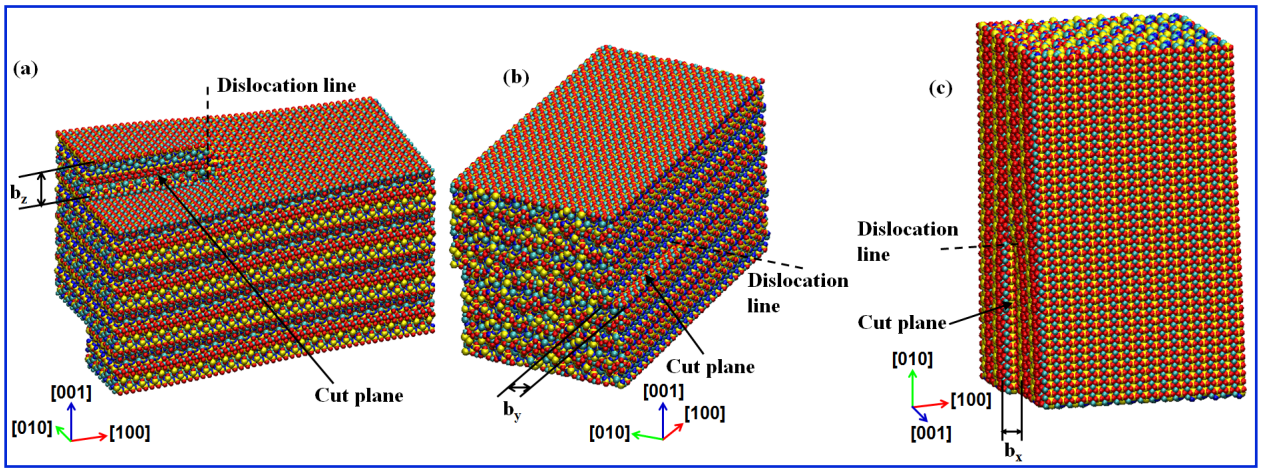

Figure 3. Atomic configurations of the super cell of tobermorite samples containing a screw dislocation with dislocation lines along (a) [001]; (b) [010]; (c) [100].

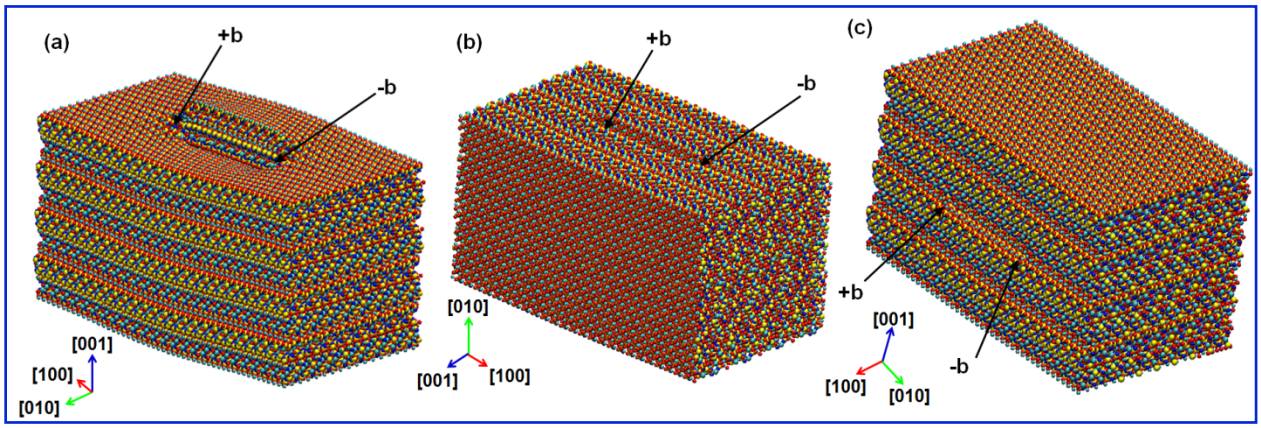

Figure 4. Atomic configurations of the super cell of tobermorite samples containing screw dislocation dipole with opposite signs, $+b$ and $-b$. The dislocation lines are along (a) [001]; (b) [010]; (c) [100].

2.2 Simulation procedure

The empirical force field CSH-FF[17, 23] has been adopted to simulate the atomic interaction in tobermorite. This force field was previously developed by our group and has been highly successful to accurately

predict the structural and mechanical properties of series of tobermorite and C-S-H families.[15, 26, 32, 40] It is also computationally much less intensive than reactive force field ReaxFF.[41] Constant volume and temperature (NVT) MD simulations are performed throughout this work. The Nose-Hoover thermostat[42-43] is used to control the temperature at constant value (298K). The velocity-Verlet algorithm[44-45] with a time step of 1 fs is used to integrate the equation of motion. Simulations are performed using the molecular dynamics program: LAMMPS package.[46]

First, the computer model with screw dislocations is allowed to relax up to 0.3 ns to reach its energy equilibrium. Once the equilibrated structure with dislocation core is obtained, shear loadings are applied on the super cell to drive the dislocation move (Figure 5a), and to compute the Peierls stress, taken here as the minimum stress leading to a core displacement. Take the sample with single screw dislocation for instance (Figure 5b), several layers of atoms on the bottom and top sides of the sample, as denoted by blue boxes, are fixed as rigid bodies. Then dipolar constant shear loadings are exerted on the fixed boundary atoms. Due to the dynamic loading, the connected regions between rigid boundary atoms and unrestraint central atoms are vulnerable to fracture. This mismatching transition stems from the fact that unrestrained atoms have no sufficient time to absorb the energy transferred from rigid boundaries. One strategy to solve this issue is to adopt quasi-static loading instead of dynamic loading. As shown in Figure 5c, the entire quasi-static loading process is divided into a direct loading region (1 ps) and a following full relax region (3 ps). The advantage of quasi-static loading is that the applied external energy can smoothly transit from the rigid boundary to the free moving internal atoms, and thus eliminating the unexpected rupture between rigid boundary and internal mobile atoms. It is worth to mention that the strain rate of the loading region is set to be 1×10^{8}/s, which has been demonstrated to be slow enough for MD simulations [14, 30]. To ensure the statistical significance of our work, a ten times slower strain rate of 1×10^{7}/s is also selected to test the strain rate effect. Simulation results indicate the mechanical properties of material including Young's modulus, strength and toughness, as well as the deformation mechanism are not

affected by the change of strain rate, which demonstrates that the current employed strain rate of 1×10^{8}/s is slow enough to produce reliable simulation results.

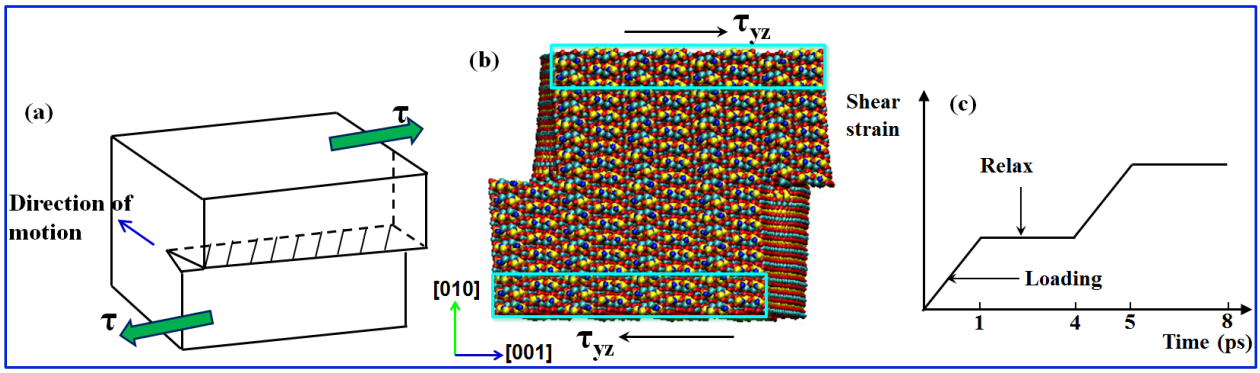

Figure 5. (a) Schematic diagram of dislocation motion under pure shear loading; (b) Cross-sectional view of sample with single screw dislocation with shear loading applied on the fixed boundaries; (c) Schematic diagram of the process of quasi-static loading.

3. Results and Discussion

3.1 Stress-strain relationships

The shear stress-strain curves for tobermorite samples with single screw dislocation, screw dislocation dipole and dislocation-free are compared in Figure 6a-c, with respect to dislocation lines along [001], [100] and [010], respectively. It can be noted from Figure 6b-c that when the dislocation lines are along [100] or [010], it can overall enhance the shear strength and elastic modulus, and the toughness of the material. Here, toughness is defined as the amount of energy a material absorbs before failure (representing the work-of-fracture), which is different from the classical "fracture toughness" with the unit of $Pa\sqrt{m}$. The work-of-fracture is the area under the stress–strain curve, which is deeply affected by gradual, "graceful fracture", whereas the fracture toughness does not incorporate this entire process.[8] The shear stress is obtained by the virial definition of stress. In the cases of pure shear on samples in which dislocation line along [001], as shown in Figure 3a, the shear stress keeps increasing till relatively large shear strains, irrespective of the introduction of screw dislocation (blue dash line in Figure 6a). Shear

stress plateaus are observed after the strain of 12.0%. With the addition of single screw dislocation or screw dislocation dipole, the shear stress seems slightly decreasing (Figure 6a). However, by tracking the deformed atomic configurations, it is found that the dislocation cannot move. Nevertheless, the connection area between rigid boundary atoms and internal free moving atoms starts rupturing (despite the use of quasi-static loading), which is believed to be responsible for the observed shear stress plateaus at high shear strain.

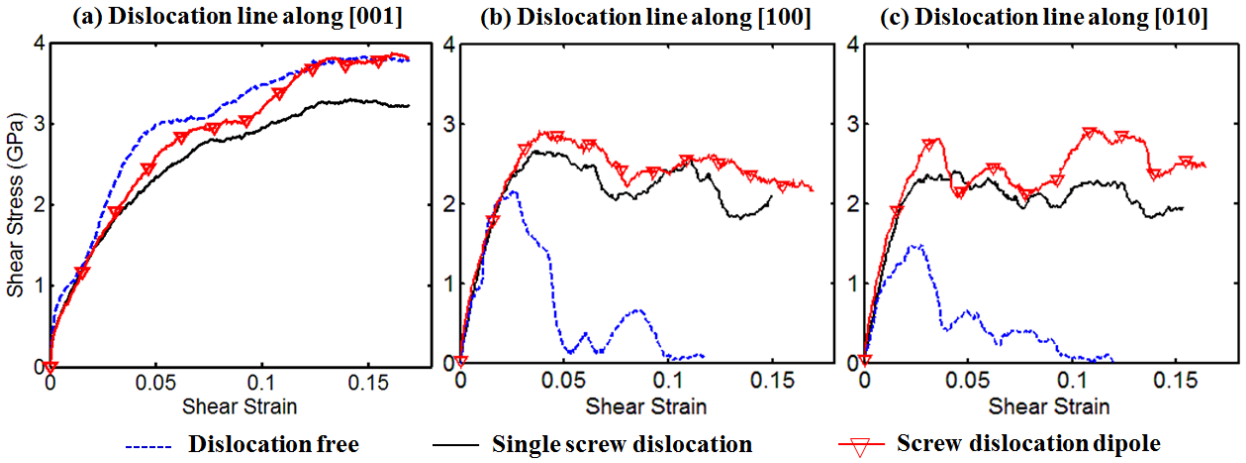

Figure 6. Comparison of stress-strain relations regarding samples with single screw dislocation, screw dislocation dipole and dislocation-free. The dislocation lines along (a) [001]; (b) [100] and (c) [010].

In the case of pure shear loading parallel to the layers, it is interesting to note that the stress-strain curves (Figure 6b,c) show different characteristic compared to that of shear along [001] direction (Figure 6a). This indicates different deformation mechanisms of the material. For the sample with single screw dislocation line along [100], the shear stress keeps increasing up to 3.8% strain (black line in Figure 6b). Then stress gradually decreases until reaches its local minimum value at strain of 8.0%. Afterwards, shear stress increases again followed by the second drop at strain of 11.0%. To identify the effect of single screw dislocation along [100] on mechanical properties of tobermorite, we performed a pure shear simulation on dislocation-free sample to make a comparison. The obtained shear stress-strain relation is plotted in Figure 6b, which shows that the stress will increase to its maximum value of 2.1 GPa at strain

of 2.0%, after which point it will drop gradually to zero. In addition, the yield shear stress, and the material toughness have been significantly reduced with respect to those of the one with single screw dislocation. This suggests that the introduction of the single screw dislocation induces a transition from a brittle nature to a ductile behavior in tobermorite.

Similar shear stress-strain responses are observed in the case of single screw dislocation line along [010] (Figure 6c), except that its yield shear stress ($\sigma_{[010]}$=2.4 GPa) is smaller than that of the case with single screw dislocation line along [100] ($\sigma_{[100]}$=2.6 GPa). The shear moduli (which can be measured in the first linear part of the stress-strain curves) in the direction parallel to the layers ([100] or [010]) is smaller than that in the direction perpendicular to the layers ([001]), consistent with the literature.[25] In the current work, the Burgers vectors along [100], [010] and [001] are 6.59 Å, 7.39 Å and 24.38 Å, respectively. The Peierls stress is sensitive to the structure of dislocation core and can be visualized as a lattice friction. Our simulations provide the Peierls stresses of samples with dislocation lines along [100], [010] as $\sigma_{[100]}$=2.6 GPa, $\sigma_{[010]}$=2.4GPa respectively. Regarding the case of dislocation of Burgers vector [001], our results indicates that these defects do not move at low or intermediate applied stress. Even for a stress larger than 3.8 GPa, no displacement of the dislocation core has been recorded. Taken also into account for the magnitude of the Burgers vector, here 24.38 Å, one can conclude that slip systems involving [001] dislocation are highly unfavorable. Moreover, in laminar structure, our Peierls stress calculations confirm that plastic behavior is restricted to the interplanar layers.

3.2 Motion of screw dislocation in (001) plane of Tobermorite

In order to elucidate the strengthening-toughening mechanism induced by the single screw dislocation in tobermorite, we track the atomic configurations of pure shear parallel to the layers, i.e., dislocation lines along [100] and [010], at various shear strains. To quantitatively study the deformation of tobermorite during shear, the displacement deviation of the individual Si atom $\left(\left|r_i^{MD} - r_i^{CB}\right|\right)$ is calculated. r_i^{MD}represents the *i*th atom's spatial vector derived by MD; and r_i^{CB} is the *i*th atom's spatial vector

computed by Cauchy-Born method.[6] Actually, the laminar structure of tobermorite implies the existence of predefined slip planes.

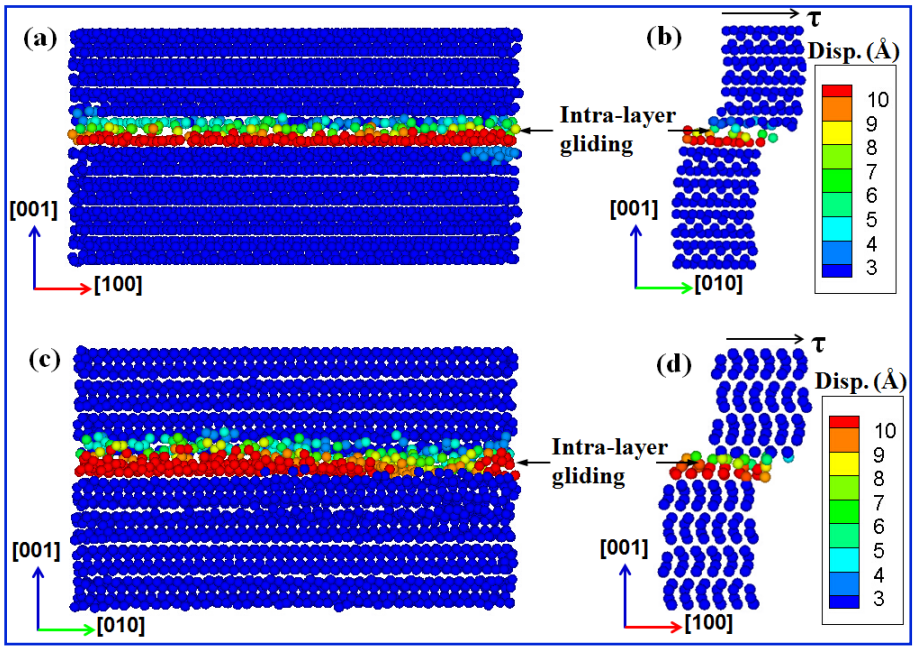

Figure 7. Snapshots of dislocation-free tobermorite at shear strain of 8.0%. The shear loadings are along (a-b) [010] and (c-d) [100]. Images are colored according to the individual displacement deviation of Si atoms in tobermorite.

Prior to investigating the structure with single screw dislocation, we first present the atomic configurations of dislocation-free tobermorite under shear loading along [100] and [010] in Figure 7a-d. The corresponding shear strain is 8.0% and the atoms are colored according to their displacement deviation. We present the cross-sectional views of a slice of computer model that are perpendicular (Figure 7a, c) and parallel (Figure 7b, d) to the shear loading.

In view of Figure 1, it is a common perception that the broad inter-laminar space is easier to slip. This is verified in Figure 7a-d and implies that the interaction between intra-laminar atoms is stronger than the interaction in between inter-laminar atoms. It is well known that the electrostatic interaction (700 - 1000 kJ/mole) is more than twenty times stronger than the hydrogen bonds (5 - 30 kJ/mole) or van der Waals

interaction.[10] In tobermorite, most of the ionic interaction is induced by Ca ions. One can note from Figure 1 that the local density of calcium ions in intra-laminar space is much higher than that in the inter-laminar space. Furthermore, the water molecules in the inter-laminar space screen the ionic chemical interactions of calcium silicates, acting as a lubricant that facilitates the molecular rearrangement in the inter-laminar space. Therefore, the intra-laminar interaction is much stronger than the inter-laminar interaction. A similar effect of water molecules on interface interaction has been reported previously.[10, 25]

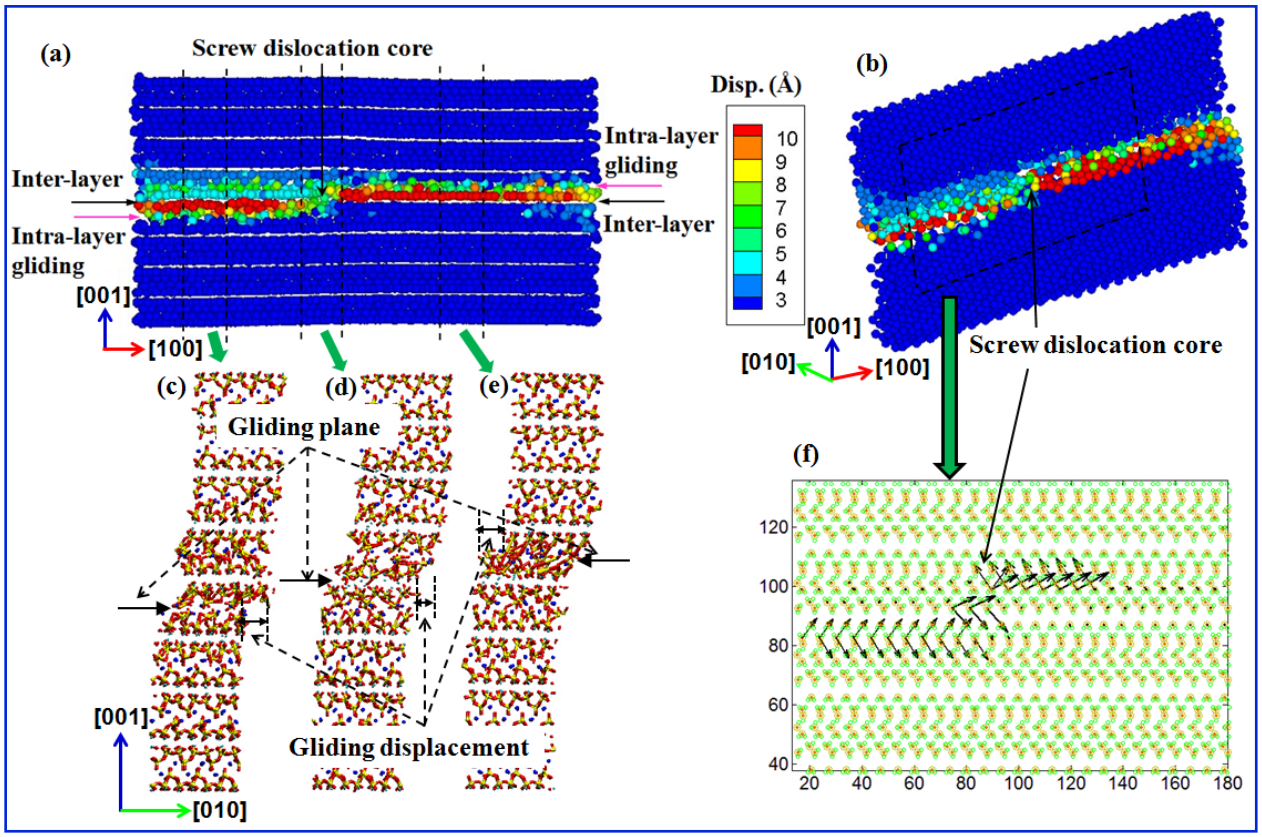

Figure 8. Atomic configurations of a slice of tobermorite with single screw dislocation line along [010] at strain of 8.0% and the corresponding differential displacement in (f). The atoms in (a) and (b) are colored by displacement deviation of Si atoms. The side cross-sectional views along [100] of all atoms at three specific locations are presented in (c-e).

With the introduction of a single screw dislocation the gliding path has been significantly influenced. Take the sample with single screw dislocation line along [010] for instance, we show the atomic

configurations of a slice of tobermorite (Figure 8c-e) at strain of 8.0% and the corresponding differential displacement (Figure 8a-b). The screw dislocation core has been denoted in Figure 8a-b, from which it is observed that with the increase of shear loading a dislocation jog with a climb around the original screw dislocation core has taken place. Particularly, the gliding planes on both sides of dislocation core are along inter-laminar spacing (Figure 8a-e), which is akin to the case of pure shear on dislocation-free tobermorite sample.

In order to deeply explore the gliding process during shear, we choose atoms at three specific locations: around dislocation core, on the left side and right side of dislocation core; and then we show the corresponding cross-sectional views along [100] in Figure 8c-e. It can be noted that on the left side (Figure 8c) and right side of dislocation core (Figure 8e) the gliding planes are along inter-laminar space. Whereas, a dominant intra-laminar gliding accompanied with slightly inter-laminar gliding is observed in the regime of screw dislocation core (Figure 8d). The gliding displacements are also labeled in Figure 8c-e. Clearly, the gliding displacement of inter-layer is larger than that of intra-layer, which once again demonstrates that intra-laminar interaction is much stronger than inter-laminar interaction.

It is believed that the local distortion of atoms near the dislocation core results in the dislocation climbing. Consequently, the inter-laminar gliding is locked around dislocation core and then the whole mechanical response is reflected as a significant increase in mechanical properties. As it will be discussed in later, the strength and toughness are improved by 26.0% and 230.0% with respect to those measured from dislocation-free samples. Therefore, the introduction of screw dislocation plays a significantly role in transiting the relatively brittle tobermorite to a ductile material. It is worth to emphasize that based on our simulation results the elastic modulus is not influenced by the screw dislocation, which is in good agreement with the theoretical analysis that elastic modulus is directly related to the elastic constant of the material. To identify and visualize the screw dislocation core and jog-pair structure, we employ differential displacement map (DDM),[32, 47] as shown in Figure 8f. The screw component of the relative displacement of the neighboring atoms produced by the dislocation is depicted as an arrow between them.

The length of each arrow is proportional to the magnitude of these components. The region of expansion of dislocation core is consistent with the dislocation jog gliding plane.

For the case of pure shear on tobermorite sample with single screw dislocation line along [100], it should be noted from Figure 6b that, the shear stress initially increases linearly in the elastic stage and subsequently enters a region characterized by a series of intermitting stress increases and drops. The post failure regime can be categorized into three stages: first, the shear stress decreases from around 2.6 GPa to 2.0 GPa as strain varies from 3.5% to 7.5%; subsequently, the shear stress steps into an increasing region until reaches its local maximum value of 2.5 GPa at strain of 11.0%; finally, shear stress drops to 1.8 GPa at strain of 13.0%. It seems that with continued loading, shear stress will increase again. In the post failure region, the three stages termed a 'valley-like' stress-strain relation is a symbol of structural rearrangement in the calcium silicate sheets. A similar 'valley-like' pattern is also observed in the case of tobermorite with single screw dislocation line along [010] (Figure 6c).

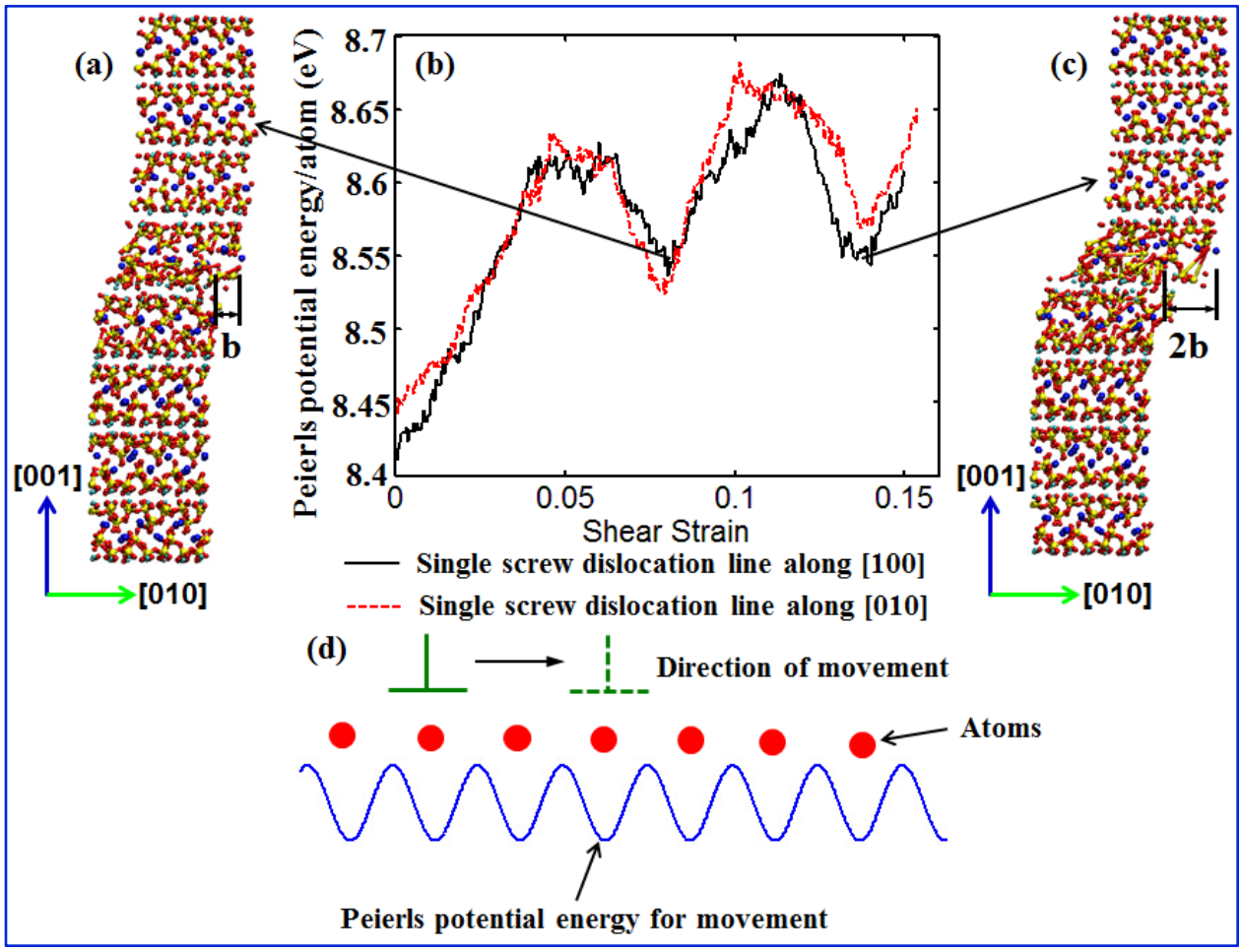

Figure 9. Peierls potential energy per atom as a function of shear strain for the cases of screw dislocation lines along [100] and [010] is plotted in (b). The snapshots (a) and (c) show the molecular configurations of the case of screw dislocation line along [100] when the Peierls potential energy is at the bottoms of valley. The cross-sectional views of the configurations is picked from the regime of screw dislocation core. (d) Schematically shows the variation of Peierls potential energy along with dislocation migration.

Peierls potential energy, which is responsible for the high lattice resistance, is an important physical property of the material.[48] Peierls potential energy defines special low-energy directions in which the dislocation prefers to lie. To this end, we analyze the energy barrier of single screw dislocation motion in tobermorite under intra-laminar pure shear. Prior to investigating the Peierls potential energy, it is instructive to track the atomic trajectories at the critical points. Since the interaction in the intra-laminar

interface is much stronger than that in the inter-laminar interface, i.e. the intra-laminar gliding around the region of screw dislocation core requires much more energy, we will focus on the atomic configurations in the regime of dislocation core.

Figure 9b shows the Peierls potential energy per atom as a function of shear strain. For the case of single screw dislocation line along [100], the cross-sectional views of atomic configuration around dislocation core when the Peierls potential energy is at the bottoms of the 'valley' are also presented in Figure 9a,c. Comparing to the shear stress-strain relations in Figure 6b, it can be easily noted that the 'valley' pattern of shear stress is in good agreement with that of Peierls potential energy. In the post failure region of Figure 6b (black line), the peaks of shear stress takes place at the strains of 4.0% and 11.0%, at which points the normalized Peierls potential energy also reaches its peak values (Figure 9b black line). Similarly, at the strains of 7.5% and 13.5%, both shear stress (Figure 6b) and normalized Peierls potential energy (Figure 9b) achieve their local minimum values.

The variation of shear stress and normalized Peierls potential energy can be interpreted as a result of intra-laminar gliding around the screw dislocation core. If the dislocation is to move, the atom has to press against the neighboring atom on one side and move away from the atom on the other side, as schematized in Figure 9d. This is clearly a situation with a higher energy, which corresponds to the first local peak at strain of 4.0% in Figure 9b. To overcome the maximum of the normalized Peierls potential energy, the shear stress has to be larger than the intrinsic critical shear stress, i.e., Peierls stress. Then it will reach the peak value at strain of 4.0% in Figure 6b. As soon as the dislocation has moved by one Burgers vector, as illustrated in the atomic configuration in Figure 9a, the shear stress and potential energy will be released instantaneously, which consequently leads to the first 'valley' of shear stress and Peierls potential energy per atom at strain of 7.5% in Figure 6b and Figure 9b, respectively. Periodically, with continued loading shear stress and Peierls potential energy will reach their second peak at strain of 11.0%, and then drop to the second 'valley' at strain of 13.5% when dislocation moves by another Burgers

vector, as shown in the atomic configuration in Figure 9c. A similar gliding process is observed in the case of pure shear on tobermorite sample with single screw dislocation line along [010].

3.3 Motion of screw dislocation dipole

In this subsection, screw dislocation dipole with dislocation lines along [001], [100] and [010] are introduced into the super cell of tobermorite, respectively. To begin, the computer models are allowed to relax to their equilibrium state. Then pure shear loadings are applied on the fixed boundaries to stimulate the motion of screw dislocation dipole. For the cases of intra-laminar shear, i.e., dislocation lines along [100] and [010], with the addition of screw dislocation dipole the shear strength and toughness are significantly improved with respect to the original defect-free structure (Figure 6b, c). This improvement is more pronounced than the previous case with single screw dislocation. However, for the sample with screw dislocation dipole with dislocation line along [001], the mechanical properties are not improved. In fact, by tracking the atomic trajectories, it is found that the yield of shear stress is due to the rupture between fixed boundary and internal mobile atoms.

First, we take an in-depth look at the normalized Peierls potential energy as shown in Figure 10. By comparing the red lines with inverted triangle in Figure 6b, c and Figure 10, at first glance, the pattern of shear stress at post failure regime appears to agree well with the pseudosinusoidal Peierls potential energy per atom. Compared to the normalized Peierls potential energy for the cases with single screw dislocation (Figure 9b), the pattern of the normalized Peierls potential energy in Figure 10 is more complex, indicating that dislocation dipoles involve more complex deformation processes.

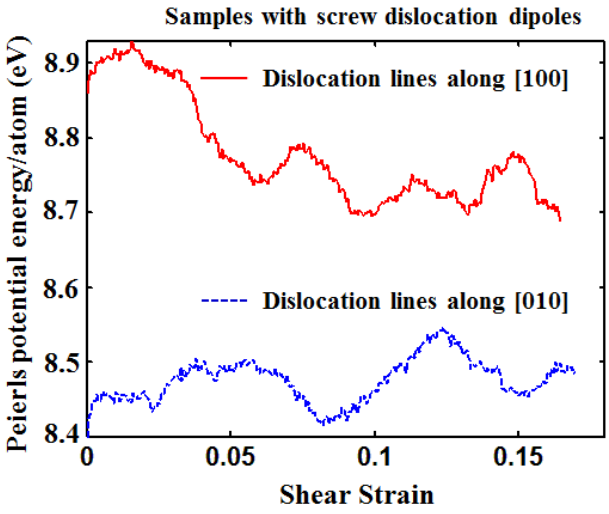

Figure 10. Peierls potential energy per atom as a function of shear strain for the cases of tobermorite with screw dislocation dipoles along [100] and [010].

To further investigate the deformation mechanisms, we show the atomic snapshots of the cases with dislocation lines along [100] and [010] at strain of 10.0% in Figure 11 and Figure 12, respectively. From Figure 11a and Figure 12a, it appears that dislocation jogs take place at the dipolar screw dislocation cores. Figure 11b-f and Figure 12b-f show the cross-sectional views of the five different slices considered here: left (Figure 11b, Figure 12b), in between (Figure 11d, Figure 12d) and right sides (Figure 11f, Figure 12f) of the dislocation dipole, as well the region around the dipolar dislocation cores (Figure 11c, e; Figure 12c, e).

For the case of dislocation line along [100], it can be noted that on the left side (Figure 11b) and right side (Figure 11f) of dislocation dipoles, gliding occurs between inter-laminar atoms. Around the dipolar screw dislocation cores, gliding dominated by intra-laminar atoms slips and is accompanied with slightly inter-laminar slip, (see double arrows in Figure 11c, e). In the region in between dislocation dipole, inter-laminar gliding, which takes place in another layer is observed (Figure 11d). Similar to the case with single screw dislocation, the local distortion around screw dislocation core prevents the original inter-laminar gliding, which consequently leads to dislocation climbing around the core. In this case, the

dipolar screw dislocations are observed to move simultaneously, which results in the 'valley' in shear stress (Figure 6b) and normalized Peierls potential energy (Figure 10).

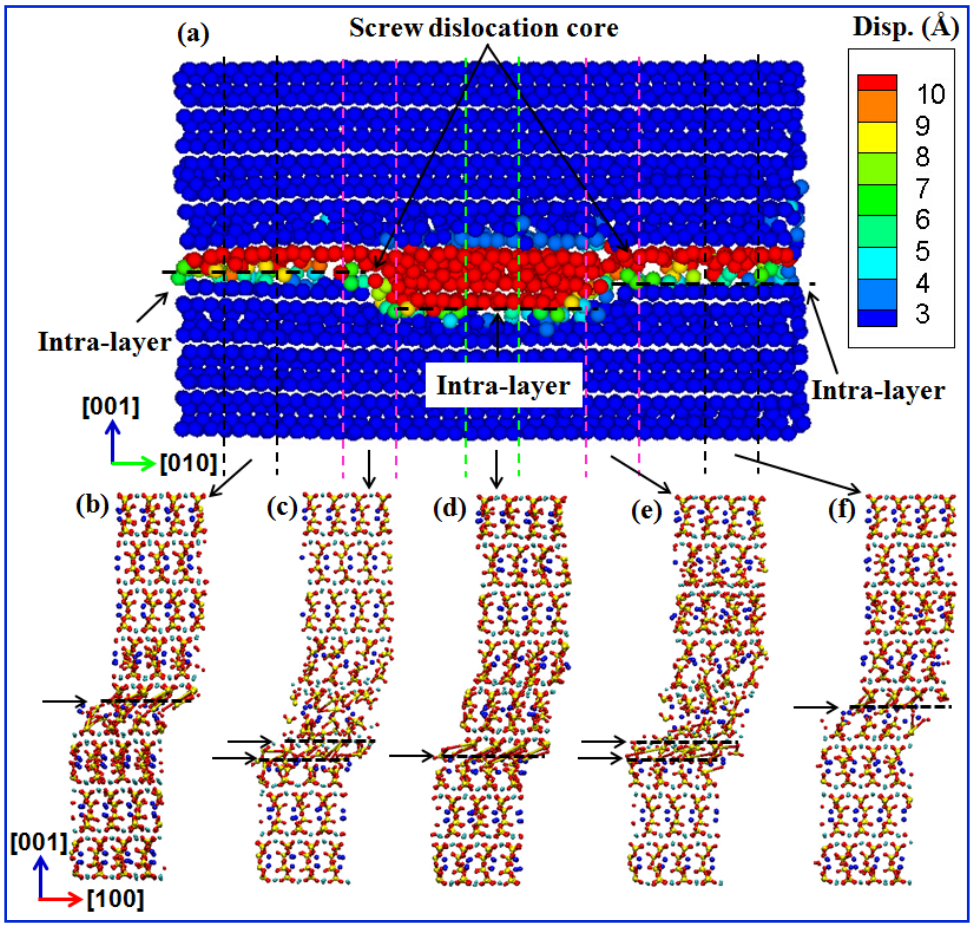

Figure 11. Atomic configurations of tobermorite with screw dislocation dipole along [100] at strain of 10.0%. The atoms in (a) are colored by their displacement deviation. (b-f) shows the cross-sectional atomic views along [010] at various locations. The dash lines and arrows in (b-f) denote the gliding planes.

Analogously, for the case of screw dislocation dipole along [010], it is observed from Figure 12a-f that inter-laminar gliding on different layers takes place on the left side (Figure 12b) and right side (Figure 12f) of screw dislocation dipole. Around the dipolar dislocation cores, intra-laminar gliding still dominates the deformation mechanism, in spite of the slightly inter-laminar gliding as denoted by double arrows and dash lines in Figure 12c, e. It is interesting to observe that only intra-laminar gliding occur in the region

between the dislocation dipole (Figure 12d), which is different from the case with screw dislocation dipole along [100]. It is worth pointing out that the intra-layer distance in the region between dislocation dipole increases due to the fact that distortion of structure makes the calcium ions in the intra-laminar space move too close. Therefore, the local intra-laminar interaction is weakened and consequently leads to the intra-laminar gliding. In addition, the intra-laminar gliding of the dipolar dislocation cores are observed not to take place simultaneously and involve much more energy accumulation and release. Both of these two important factors are responsible for the multiple 'valleys' and the large magnitude of variation in shear stress (Figure 6c) and normalized Peierls potential energy (Figure 10). Consequently, shear strength and material toughness are significantly improved (Figure 13), again pointing out to the dislocation-induced brittle to ductile transition. Note that the dislocations typically form based on the least resistance for formation. The formation of cut planes in the intra laminar involved breaking covalent bonds, which entails a lot more energy and thus it does not occur. As such, the discussed brittle to ductile transitions in this manuscript corresponds to inter- laminar dislocations.

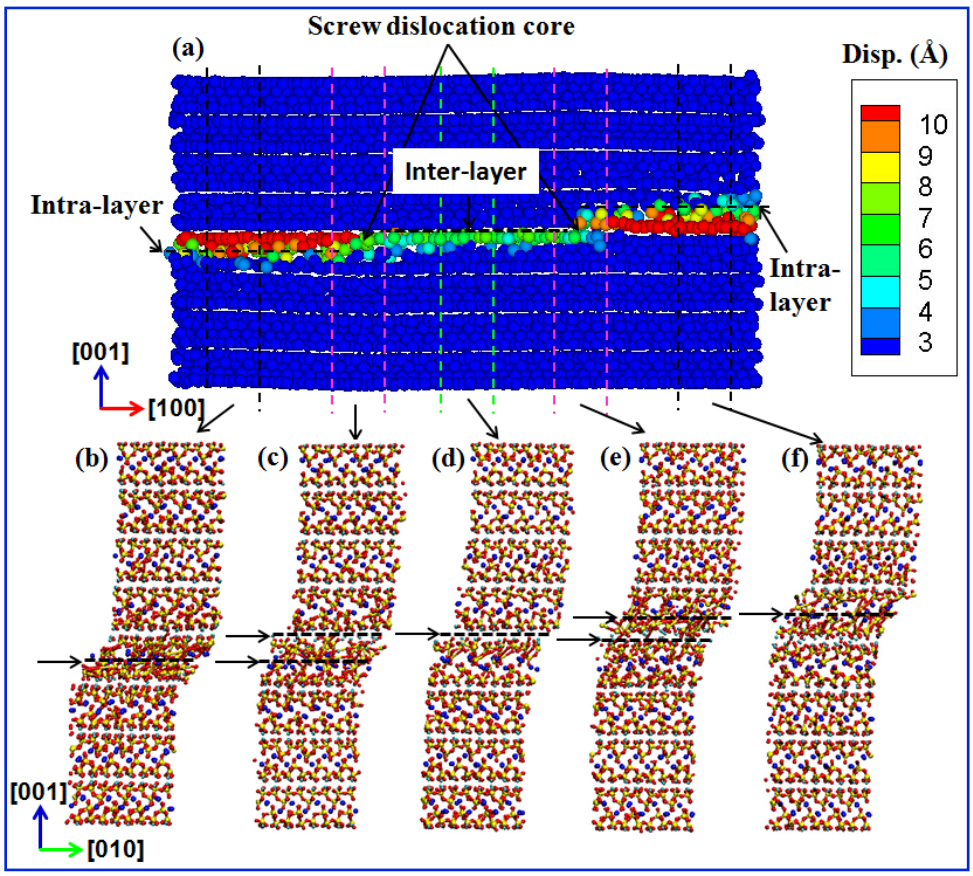

Figure 12. Atomic configurations of tobermorite with screw dislocation dipole along [010] at strain of 10.0%. The atoms in (a) are colored by their displacement deviation. (b-f) show the cross-sectional atomic views along [100] at five various locations. The dash lines and arrows in (b-f) denote the gliding planes.

4. Conclusion

We used MD simulations to investigate the effects of screw dislocation on the mechanical response of tobermorite under pure shear. We categorized the samples with screw dislocations into two classes: one with dislocation line perpendicular to the layers (along [001]) and one with dislocation line parallel to the layers (along [100] or [010]). Our results indicate that the sample with screw dislocation lines parallel to the layers can significantly improve the mechanical properties (Figure 13a-b). From Figure 13a-b, we infer that shear strength and toughness have been significantly improved, ~100% and ~500% respectively, due to existence of screw dislocation of Burgers vector [100] or [010] and screw dislocation dipole.

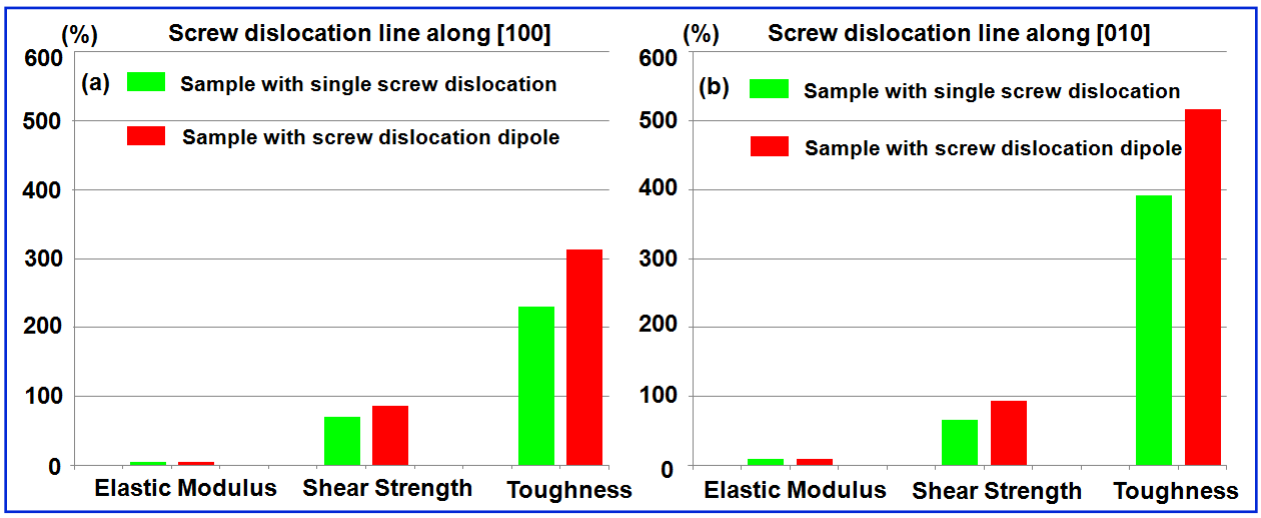

Figure 13. Comparisons of the effects of single screw dislocation and dislocation dipole on elastic modulus, shear strength and toughness. The screw dislocation lines are along (a) [100] and (b) [010]. Note that the vertical axis stands for the percentage of increased mechanical properties with respect to those measured from the defect-free tobermorite.

Through tracking the atomic trajectories, we found that inter-laminar gliding dominates the deformation process of defect-free tobermorite under shear loading. The water molecules in the inter-laminar spacing act as a lubricant that facilitates the sliding between adjacent particles. With the introduction of single and dipolar screw dislocation, a dislocation jog and climbing is observed around the dislocation core, respectively. While in the case of single dislocation, a dominant intra-laminar gliding accompanied by a slightly inter-laminar gliding is identified around the core region, inter-laminar gliding is found to be the dominant dislocation motion in the case of dipolar dislocation. In the latter case, intra-laminar gliding is observed in the region between dipolar dislocation cores when the screw dislocation dipole line is along [010]. We also analyzed the 'valley-like' pattern of Peierls potential energy and confirm that it is in good agreement with shear stress in the post failure regime.

Owing to the local distortion of displacement around screw dislocation core, the original straight inter-laminar gliding is interrupted. Screw dislocation core acts as a local lock to impede initial slide, and also

it is a junction that transits inter-laminar gliding from one layer to another layer. The dislocation jog formation energy, i.e., local maximum Peierls potential energy, is responsible for the improvement of mechanical properties. This research provides new physical insights for developing new strategies for brittle-to-ductile transition of complex brittle materials such as tobermorite. To our knowledge, this work is the first report of atomistic-scale analysis of the effects of single screw dislocation and screw dislocation dipole on mechanical properties of C-S-H crystals. Our findings on strengthening-toughening mechanisms in this paper can potentially provide new hypotheses and design guidelines for developing strong and tough C-S-H and other complex materials.[27, 49-52.]

Acknowledgements

We acknowledge support from National Science Foundation (NSF) Grant Nos. CMMI-1235522 and 1346506. The use of supercomputer machines for this work was supported in part by National Insitutes of Health Award No. NCRR S10RR02950 and an IBM Shared University Research (SUR) Award in partnership with CISCO, Qlogic, and Adaptive Computing, and in part by the Data Analysis and Visualization Cyber infrastructure funded by NSF under Grant No. OCI-0959097.

Reference

1. Bouville, F.; Maire, E.; Meille, S.; Van de Moortèle, B.; Stevenson, A. J.; Deville, S., Strong, Tough and Stiff Bioinspired Ceramics from Brittle Constituents. *Nat. Mater.* **2014,** *13* (5), 508-514.
2. Li, J.; Suo, Z.; Vlassak, J. J., Stiff, Strong, and Tough Hydrogels with Good Chemical Stability. *J. Mater. Chem. B* **2014,** *2* (39), 6708-6713.
3. Ritchie, R. O., The Conflicts between Strength and Toughness. *Nat. Mater.* **2011,** *10* (11), 817-822.
4. Porter, M. M.; McKittrick, J., It's Tough to Be Strong: Advances. *Am. Ceram. Soc. Bull* **2014,** *93*, 18-24.
5. Hofmann, D. C.; Suh, J.-Y.; Wiest, A.; Lind, M.-L.; Demetriou, M. D.; Johnson, W. L., Development of Tough, Low-Density Titanium-Based Bulk Metallic Glass Matrix Composites with Tensile Ductility. *Proc. Natl. Acad. Sci.* **2008,** *105* (51), 20136-20140.
6. Abdolhosseini Qomi, M. J.; Ulm, F. J.; Pellenq, R. J. M., Evidence on the Dual Nature of Aluminum in the Calcium-Silicate-Hydrates Based on Atomistic Simulations. *J. Am. Ceram. Soc.* **2012,** *95* (3), 1128-1137.
7. Kalinichev, A. G.; Kirkpatrick, R. J., Molecular Dynamics Modeling of Chloride Binding to the Surfaces of Calcium Hydroxide, Hydrated Calcium Aluminate, and Calcium Silicate Phases. *Chem. Mater.* **2002,** *14* (8), 3539-3549.

8. Sakhavand, N.; Shahsavari, R., Universal Composition–Structure–Property Maps for Natural and Biomimetic Platelet–Matrix Composites and Stacked Heterostructures. *Nat. Commun.* **2015,** *6, 6523*.
9. Franceschini, A.; Abramson, S.; Mancini, V.; Bresson, B.; Chassenieux, C.; Lequeux, N., New Covalent Bonded Polymer–Calcium Silicate Hydrate Composites. *J. Mater. Chem.* **2007,** *17* (9), 913-922.
10. Zhang, N.; Chen, Y., Molecular Origin of the Sawtooth Behavior and the Toughness of Nacre. *Mater. Sci. Eng., C* **2012,** *32* (6), 1542-1547.
11. Sun, J.; Bhushan, B., Hierarchical Structure and Mechanical Properties of Nacre: A Review. *Rsc Advances* **2012,** *2* (20), 7617-7632.
12. Shahsavari, R. Hierarchical Modeling of Structure and Mechanics of Cement Hydrate. Massachusetts Institute of Technology, **2011**.
13. Zhang, N.; Deng, Q.; Hong, Y.; Xiong, L.; Li, S.; Strasberg, M.; Yin, W.; Zou, Y.; Taylor, C. R.; Sawyer, G., Deformation Mechanisms in Silicon Nanoparticles. *J. Appl. Phys.* **2011,** *109* (6), 063534.
14. Zhang, N.; Zaeem, M. A., Competing Mechanisms between Dislocation and Phase Transformation in Plastic Deformation of Single Crystalline Yttria-Stabilized Tetragonal Zirconia Nanopillars. *Acta Materialia* **2016,** *120*, 337-347.
15. Qomi, M. A.; Krakowiak, K.; Bauchy, M.; Stewart, K.; Shahsavari, R.; Jagannathan, D.; Brommer, D.; Baronnet, A.; Buehler, M.; Yip, S., Combinatorial Molecular Optimization of Cement Hydrates. *Nat. Commun.* **2014,** *5, 4960*.
16. Bauchy, M.; Laubie, H.; Qomi, M. A.; Hoover, C.; Ulm, F.-J.; Pellenq, R.-M., Fracture Toughness of Calcium–Silicate–Hydrate from Molecular Dynamics Simulations. *J. Non-Cryst. Solids* **2015,** *419*, 58-64.
17. Shahsavari, R.; Pellenq, R. J.-M.; Ulm, F.-J., Empirical Force Fields for Complex Hydrated Calcio-Silicate Layered Materials. *PCCP* **2011,** *13* (3), 1002-1011.
18. Raki, L.; Beaudoin, J.; Alizadeh, R.; Makar, J.; Sato, T., Cement and Concrete Nanoscience and Nanotechnology. *Materials* **2010,** *3*, 918-942.
19. Merlino, S.; Bonaccorsi, E.; Armbruster, T., Tobermorites: Their Real Structure and Order-Disorder (Od) Character. *Am. Mineral.* **1999,** *84*, 1613-1621.
20. Richardson, I., The Calcium Silicate Hydrates. *Cem. Concr. Res.* **2008,** *38* (2), 137-158.
21. Thomas, J. J.; Jennings, H. M.; Allen, A. J., Relationships between Composition and Density of Tobermorite, Jennite, and Nanoscale Cao− Sio2− H2o. *J. Phys. Chem. C* **2010,** *114* (17), 7594-7601.
22. Merlino, S.; Bonaccorsi, E.; Armbruster, T., The Real Structure of Tobermorite 11å Normal and Anomalous Forms, Od Character and Polytypic Modifications. *Eur. J. Mineral.* **2001,** *13* (3), 577-590.
23. Shahsavari, R.; Buehler, M. J.; Pellenq, R. J. M.; Ulm, F. J., First‐Principles Study of Elastic Constants and Interlayer Interactions of Complex Hydrated Oxides: Case Study of Tobermorite and Jennite. *J. Am. Ceram. Soc.* **2009,** *92* (10), 2323-2330.
24. Hou, D.; Zhao, T.; Ma, H.; Li, Z., Reactive Molecular Simulation on Water Confined in the Nanopores of the Calcium Silicate Hydrate Gel: Structure, Reactivity, and Mechanical Properties. *J. Phys. Chem. C* **2015,** *119* (3), 1346-1358.
25. Manzano, H.; Masoero, E.; Lopez-Arbeloa, I.; Jennings, H. M., Shear Deformations in Calcium Silicate Hydrates. *Soft Matter* **2013,** *9* (30), 7333-7341.
26. Jalilvand, S.; Shahsavari, R., Molecular Mechanistic Origin of Nanoscale Contact, Friction, and Scratch in Complex Particulate Systems. *ACS Appl. Mater. Interfaces* **2015,** *7* (5), 3362-3372.
27. Zhang, N.; Shahsavari, R., Balancing Strength and Toughness of Calcium-Silicate-Hydrate Via Random Nanovoids and Particle Inclusions: Atomistic Modeling and Statistical Analysis. *J. Mech. Phys. Solids* **2016,** *96*, 204-222.
28. Choudhury, R.; Gattinoni, C.; Makov, G.; De Vita, A., Molecular Dynamics Studies of the Dissociated Screw Dislocation in Silicon. *J. Phys.: Condens. Matter* **2010,** *22* (7), 074210.
29. Mordehai, D.; Clouet, E.; Fivel, M.; Verdier, M., Introducing Dislocation Climb by Bulk Diffusion in Discrete Dislocation Dynamics. *Philos. Mag.* **2008,** *88* (6), 899-925.

30. Zhang, N.; Chen, Y., Nanoscale Plastic Deformation Mechanism in Single Crystal Aragonite. *Journal of Materials Science* **2013,** *48* (2), 785-796.
31. Yadav, S.; Ramprasad, R.; Misra, A.; Liu, X.-Y., Core Structure and Peierls Stress of Edge and Screw Dislocations in Tin: A Density Functional Theory Study. *Acta Mater.* **2014,** *74*, 268-277.
32. Shahsavari, R.; Chen, L., Screw Dislocations in Complex, Low Symmetry Oxides: Core Structures, Energetics, and Impact on Crystal Growth. *ACS Appl. Mater. Interfaces* **2015,** *7* (4), 2223-2234.
33. Walker, A.; Carrez, P.; Cordier, P., Atomic-Scale Models of Dislocation Cores in Minerals: Progress and Prospects. *Mineral Mag.* **2010,** *74* (3), 381-413.
34. Kabir, M.; Lau, T. T.; Rodney, D.; Yip, S.; Van Vliet, K. J., Predicting Dislocation Climb and Creep from Explicit Atomistic Details. *Phys. Rev. Lett.* **2010,** *105* (9), 095501.
35. Chisholm, M. F.; Kumar, S.; Hazzledine, P., Dislocations in Complex Materials. *Science* **2005,** *307* (5710), 701-703.
36. Proville, L.; Ventelon, L.; Rodney, D., Prediction of the Kink-Pair Formation Enthalpy on Screw Dislocations in A-Iron by a Line Tension Model Parametrized on Empirical Potentials and First-Principles Calculations. *Phys. Rev. B* **2013,** *87* (14), 144106.
37. Wang, G.; Strachan, A.; Cagin, T.; Goddard, W. A., Molecular Dynamics Simulations of 1/2 a< 1 1 1> Screw Dislocation in Ta. *Mater. Sci. Eng., A* **2001,** *309*, 133-137.
38. Volterra, V. In *Sur L'équilibre Des Corps Élastiques Multiplement Connexes*, Annales scientifiques de l'Ecole Normale superieure, Société mathématique de France: **1907**; pp 401-517.
39. Friedel, J., *Dislocations: International Series of Monographs on Solid State Physics*. Elsevier: **2013**.
40. Shahsavari, R.; Chen, L.; Tao, L., Edge Dislocations in Dicalcium Silicates: Experimental Observations and Atomistic Analysis. *Cem. Concr. Res.* **2016,** *90*, 80-88.
41. Van Duin, A. C.; Dasgupta, S.; Lorant, F.; Goddard, W. A., Reaxff: A Reactive Force Field for Hydrocarbons. *J. Phys. Chem. A* **2001,** *105* (41), 9396-9409.
42. Woodcock, L.-V., Isothermal Molecular Dynamics Calculations for Liquid Salts. *Chem. Phys. Lett.* **1971,** *10* (3), 257-261.
43. Nosé, S., A Unified Formulation of the Constant Temperature Molecular Dynamics Methods. *J. Chem. Phys.* **1984,** *81* (1), 511-519.
44. Verlet, L., Computer" Experiments" on Classical Fluids. I. Thermodynamical Properties of Lennard-Jones Molecules. *Phys. Rev.* **1967,** *159* (1), 98.
45. van Gunsteren, W. F.; Berendsen, H. J., Computer Simulation of Molecular Dynamics: Methodology, Applications, and Perspectives in Chemistry. *Angew. Chem., Int. Ed. Engl.* **1990,** *29* (9), 992-1023.
46. Plimpton, S., Fast Parallel Algorithms for Short-Range Molecular Dynamics. *J. Comput. Phys.* **1995,** *117* (1), 1-19.
47. Gordon, P.; Neeraj, T.; Li, Y.; Li, J., Screw Dislocation Mobility in Bcc Metals: The Role of the Compact Core on Double-Kink Nucleation. *Modell. Simul. Mater. Sci. Eng.* **2010,** *18* (8), 085008.
48. Weinberger, C. R.; Tucker, G. J.; Foiles, S. M., Peierls Potential of Screw Dislocations in Bcc Transition Metals: Predictions from Density Functional Theory. *Phys. Rev. B* 2013, *87* (5), 054114.
49. Moghaddam, H.E.; Hejazi V.; Hwang, S.; Sreeparasad, ST.; Miller, J.; Shi, B.; Zhou, S.; Rusakova, I.; Alizadeh, A.; Whitmire, K.; Shahsavari, R., Morphogenesis of Cement Hydrate, J*ournal of Materials Chemistry A*, **2016**, DOI: DOI: 10.1039/C6TA09389B
50. Shahsavari, R.; Chen, L.; Tao, L., Structure, Energetic and Impact of Screw Dislocations in Tricalcium Silicates, *Journal of American Ceramics Society*, **2016**, 1-9.
51. Kim, N.; Metzger, A.; Hejazi, V.; Li, Y.; Kovalchuk, A.; Lee, S.K.; Ye, R.; Mann, J.; Kittrell, C.; Shahsavari, R.; Tour, J.M., Microwave Heating of Functionalized Graphene Nanoribbons in Thermoset Polymers for Wellbore Reinforcement, *ACS Applied Materials and Interfaces*, **2016**, 8, 12985-12991.

52. Sakhavand, N.; Muthuramalingam, P.; Shahsavari, R., Toughness Governs the Rupture of Interfacial H-bond Assemblies at a Critical Length Scale in Hybrid Materials, *Langmuir*, **2013**, 29 (25), 8154-163.

Table of Content Graphics